Probing Trees Annual Rings For The Effects of Volcanic Eruptions Using PIXE

Master's Thesis
Physics

(Materials Research)

University of Helsinki

Department of Physics

ADIO, LUQMON O.

Date: April 23rd, 2019
Student Number: 014610978
Supervisors: Mizohata Kenichiro
Jyrki Raisanen

HELSINGIN YLIOPISTO
HELSINGFORS UNIVERSITET
UNIVERSITY OF HELSINKI
MATEMAATTIS-LUONNONTIETEELLINEN TIEDEKUNTA
MATEMATISK-NATURVETENSKAPLIGA FAKULTETEN
FACULTY OF SCIENCE

Tiedekunta – Fakultet – Faculty	Koulutusohjelma – Utbildningsprogram– Degree programme
Faculty of Science	Department of Physics (Materials Research)

Tekijä – Författare – Author

Luqmon Adio O.

Työnnimi – Arbetets titel – Title

Probing Trees Annual Rings For The Effects of Volcanic Eruptions Using PIXE

Työnlaji – Arbetets art – Level	Aika – Datum – Month and year	Sivumäärä – Sidoantal – Number of pages
Master's Thesis	April 2019	43

Tiivistelmä – Referat – Abstract

Particle Induced X-ray Emission (PIXE) was originally introduced as an ion-beam analytical technique in Lund in the 1970s and has since then been part of the available techniques in many laboratories around the world. The external beam PIXE set-up is used in probing the annual tree rings. The goal is to see the effects of volcanic eruption activities from the perspectives of tree plants here in Finland. In the theory part, I tried to include the description of how volcanoes are formed and created with a bit of volcanic activity history, the growth metabolism mechanism in tree plants and characteristics x-ray productions.

The two tree sample used for this experiment were gotten from two different regions of Finland. The first tree is a Pine tree from Parikkala(a small place near Savolinna) in the south-eastern part of Finland and the second tree is a Spruce tree from Pielavesi (place near Kuopio) in the central part of Finland. These samples were carefully prepared for ionisation.

The collected spectra data were analysed in a software called PyMCA. PyMCA has been developed by the Software Group of the European Synchrotron Radiation Facility (ESRF). PyMCA is a ready to use and in many aspects state-of-the-art, set of applications implementing most of the needs of X-ray fluorescence data analysis. PyMCA is use to interpret X-ray fluorescence spectra from a diverse array of samples.

Avainsanat – Nyckelord – Keywords

PIXE, exit window, beam current measurement, PyMca, MCA .

Säilytyspaikka – Förvaringställe – Where deposited

Muitatietoja – Övriga uppgifter – Additional information

Contents

1 Introduction

1.1 What PIXE is about briefly

The acronym PIXE, simply stands for Particle Induced X-ray Emission. It is one of the various types of an ion beam analysis (IBA) technique that is a very powerful, yet non-destructive, technique used in the determination of the elemental constituents and composition of a material or sample. When a material is irradiated by an ion beam, atomic interactions occur that give off electromagnetic radiation of wavelengths in the X-ray part of the electromagnetic spectrum specific to that element. The letter ”P” in PIXE, can be interchangeably used to mean ”Particle” or ”Proton” depending on the kind of projectile used to create this irradiation. Main idea of the PIXE method is to excite atoms of the specimen with the ion beam of protons, alpha particles or heavy ions and detect characteristic x-rays, which are emitted by the target atoms when they are de-excited. For the the spectrum that is measured with for example a semiconductor x-ray detector, the area under the characteristic x-ray peaks is proportional to the concentration of the different elements in the sample.

Different ranges of samples such as solids (plastics, papers or metals); powdered materials (fly ash, activated carbon, catalysts, and corrosion products) liquids (oils, process waters, and solutions) and aerosol filters (thin film membrane samples) are assayed by PIXE. Also thus are in Archaeological, medical and in environmental materials[1]. PIXE is a very highly sensitive and simple method and several tens of μg of sample is enough for PIXE experiments[2]

Electrons were commonly used as projectiles in early days of PIXE method. In the year 1912, James Chadwick, was able to demonstrate that Heavier particles used as projectiles give x-ray emission. Chadwick used an alpha particles from radioactive source as projectiles in his demonstration[3]. This was however a long time prior to the use of accelerators and the used beam intensity was too low for an analysis like PIXE.

The use of accelerators from 1950s ushered in a new adventure in the area of nuclear physics research, the main reason for it was because the X-ray background observed in nuclear research works. There were so many works on this as a result. This gave a lot of new information about the role of particle’s atomic number and energy in the X-ray production cross sections. It was already known from the theory that heavy charged particles produce much less amount of bremsstrahlung radiation than does by the very light particles such as electrons. Reason for this low bremsstrahlung radiation is the rate of deceleration experienced by projectile in the specimen which definitely is much smaller for ions than for electrons, which is mainly due to there the variance in there sizes. when a proton beam is used as a projectile the contributor of the bremsstrahlung are the secondary electrons[4].

Particle Induced X-ray Emission (PIXE) was originally introduced as an ion-beam analytical technique in Lund in the 1970s[5] and has since then been part of the available techniques in many laboratories around the world. PIXE-analysis can be

carried out using both a mm-sized beam as well as with a scanning focused microbeam. By combining PIXE with additional nuclear scattering and reaction techniques, the elemental analytical capability will be extended to approach the full periodic table[6].

The full range of ion beams analytical techniques includes many different methods based on similar principles: firstly, a beam of MeV ions is aimed at the sample. These projectiles penetrate into the sample losing energy continuously at a well-known rate(stopping power). Along their trajectories there is the chance for collisions with nuclei and with electrons. Secondly, as a result of these collisions, the products of these interactions are emitted from the sample, with probabilities determined by the respective interaction cross-sections, and are finally measured and collected as spectra carrying information on the chemical composition of the sample and the elemental depth distributions.

1.1.1 Other IBA Methods

Here, I try to discuss other methods of the IBA that can also be used alongside with PIXE to obtain a more comprehensive analysis.

– In RBS (Rutherford backscattering spectrometry) one records projectiles elastically backscattered from nuclei of sample atoms. The measured energy depends on the mass of the target nucleus (and thus on the element or isotope) and also on the depth of the scattering event beneath the surface.

– In ERDA (elastic recoil detection analysis) is also based on elastic scattering. One records the target nuclei recoiled by the scattering of projectiles. The measured energy depends on the mass of the recoil and on the depth of the scattering event.

– In NRA (nuclear reaction analysis) relies on the measurement of the products of nuclear reactions between projectile and target nuclei. The recorded energy of the products gives information on the specific target nucleus and, in general on the depth of the reaction event.

In addition, there are many other techniques, as for example particle induced gamma ray emission (PIGE), charged particle activation analysis (CPAA), scanning transmission ion microscopy (STIM), Sonoluminescence and ion beam induced charge imaging (IBIC). Many of these techniques may be applied simultaneously. For example, PIXE, RBS, ERDA, NRA and PIGE instrumentation may all be installed in the same vacuum chamber and applied at the same time[7].

1.2 Aim of This Thesis

The aim of this thesis is to research and document the external beam PIXE set-up usage in probing the annual tree rings. The goal is to see the effects of volcanic eruption activities from the perspectives of tree plants here in Finland. The theory part includes description of how volcanoes are formed and created with a bit volcanic

activity history, the growth metabolism mechanism in tree plants, characteristics x-ray productions, the formation of the background spectrum and quantitative analysis. In the experimental section of this work has in it the description of the setup of the whole experiment and all the required measurements technicalities are explained in detail. Also, PIXE measurements on wood samples and results are described.

The aim of this research is to see if we can observe the effect of volcanic activities on tree plants here in Finland from different locations and then observe the effects created.

1.3 Aim of This Research

The major motive in physics department for this research was to develop existing PIXE set-up so that it is suitable for extensive research of any kind of material sample. Numerous Papers about the new external beam PIXE set-up with large area SiN window has been submitted and published[8].

Perfuming this experiment can be a very good learning tool for students doing their studies in advance laboratory exercises and working on their personal study projects for degrees and postgraduate degrees.

The research in this area has been used to analyse the elemental concentration of archaeological findings in different regions of Europe, most especially in the Northern region. With these observations, archaeologists can determine the provenance of these neolithic stone age pottery pieces and with that determine the migration of human population in northern Europe at that time. Presentation about the analysis of the provenance results was held in International Symposium on Archaeometry in Los Angeles in May 2014[9].

2 Theory

This section is divided into three parts the first is the brief physical explanation of ionisation, de-excitation process by characteristic x-ray emission and background emissions(bremsstrahlung). The second part is what the volcano is about, how it occurs and what is associated with it. The third part is about the metabolism of tree plants and its growth.

2.1 Collision Theory of Ions on Target Atoms

In the quest to understand atomic level physical rules, behaviours and characteristics, collisions of ions with atoms define one of the most actively researched areas of atomic physics. The design and construction of accelerators needed for these experiments In the last few decades, as well as the theoretical description of ion-atom collisions has advanced considerably. In an ion-atom collision, an ion or atom with velocity v or energy E impinges on a target, which is usually at rest in the laboratory system. Of all the various fundamental interaction processes occurring during ion-atom collision, the production of core vacancy states, in which one or more of the relatively tightly bound target atom's electrons is removed. This leaves the target's atom in an excited state which is highly unstable too. The decay of such highly excited systems is usually studied through the measurements of electrons, photons, or both, emitted in subsequent relaxation of the state. Study of all these processes provides a better window of understanding into the ion-atom interactions and gives us important information about the (fundamentally many-body) collision interactions themselves, the nature of transient excited states formed, and the relaxation processes by which the ions and atoms return to neutral or charged ground states.

2.1.1 De-excitation of Atoms With Vacant Inner Shell

An excited atom with vacancy in its inner shell return to ground state through various processes which can be classed into two different groups. these groups are:

(i) Non-radiative transition and
(ii) Radiative transition

These two are illustrated in the Figure 2 below.

Non-radiative transition:

During this process of Non-radiative transition, as implied in the name, the inner-shell vacancy is filled by an electron from the outer shell of the atom and the available energy of transition is used to eject an electron from another loosely bound higher shell. This ejected electron is called the Auger electron and this whole process is called Auger process. The term "Auger transition" is used for transitions in which a single vacancy within an atomic shell leads to creating two other vacancies in principal shells other than the original shell containing the initial vacancy. However, in the case

of transitions, where one of the two vacancies produced in such decay process is in a different sub-shell of the same principal shell containing the initial vacancy, are called as Coster-Kronig (CK) transitions. Several works and publications have been made on this subject[10].

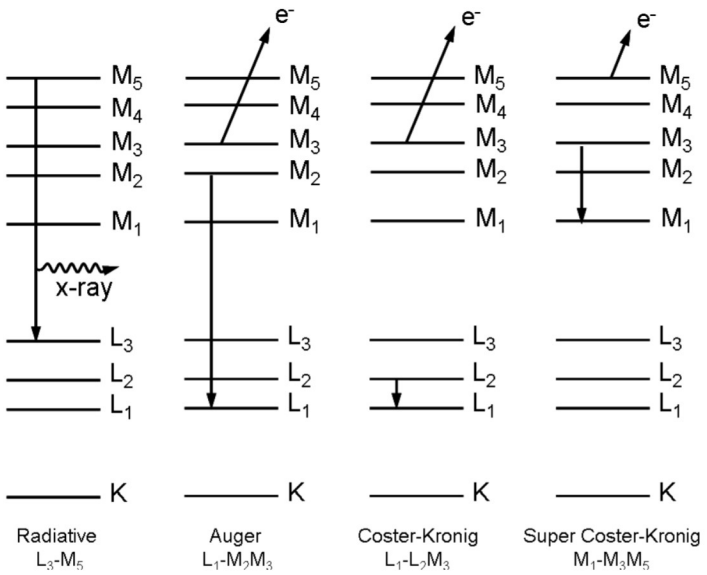

Figure 1: Radiative and Non-radiative transitions.

Radiative transition:

This transition is radiative, the inner-shell vacancy is refilled by an electron from outer shell thereby shifting the vacancy of the inner shell to the outer shell and the difference in energy level is released in form of x-rays. The emission of x-rays is governed by selection rules for allowed electric dipole $E1$ transitions. All the X-ray transitions that contradicts the electric dipole selection rules are said to be forbidden and have much lower transition rates [11]. The dipole-allowed x-ray transitions to the K and L shells of single-vacancy atoms are shown in Figure 2. The probability that an inner vacancy will be filled in an x-ray transition is known as the fluorescence yield (ω). Thus the fluorescence yield is the ratio of the number of x-rays emitted to the number of total vacancies created in that shell.

The de-excitation of K-shell vacancies is simple and straightforward just because there is only one possible initial state. However, the de-excitation process is complicated for L-shell or higher shell vacancies by two different factors. The first of these factors is that shells higher than the K-shell consist of more than one sub-shell and the de-excitation process depends on how the sub-shells are ionised, since different methods of ionization will yield different primary vacancy distributions. The second

reason is that The original vacancies in a shell may rearrange through Coster- Kronig transitions. Various data based upon different theoretical models are available in different paper publication for the radiative emission rate of different shells [12,13,14].

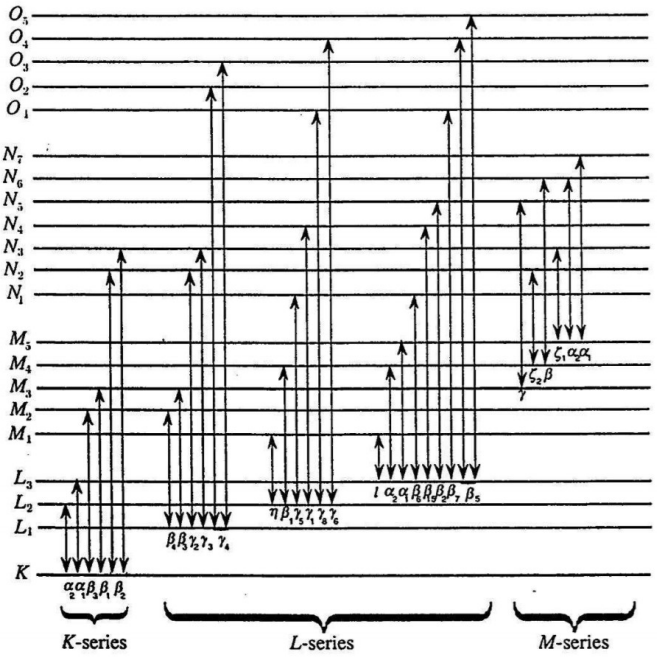

Figure 2: Schematic diagram of the generation of various X-ray lines from different electronic transitions.

Almost all of inner-shell ionisation cross section data is obtained out of total x-ray production cross sections, since x-ray detector systems are less complex than those of Auger. The x-ray spectrum associated with energetic ion-atom collision can be detected and analysed experimentally by means of conventional nuclear instruments, these instruments are; appropriate detector, pre-amplifier, amplifier, voltage bias supply, and multi-channel analyser. A high resolution detector is often required. Usually lithium drifted Silicon (Si(Li))(very good for detecting trace elements) and high purity germanium (HPGe) detectors (very good for detecting heavier atoms) offer proper and resilient detection capability that suits the complex nature of x-ray spectra. Major reason why they are widely utilised for such measurements. Data is always recorded and transferred from detector system to a computer using suitable network procedure in order to carry out the analysis that involves the analytical fitting of the x-ray spectrum and peak area determinations.

2.2 Particle Induced X-ray Emission (PIXE)

As briefly explained in the previous section, PIXE is the process where x-rays are induced by the impact of energetic ions due to the Coulomb interaction between the incident ion and inner-shell bound electron, giving rise to vacancy in the target atom. This created vacancy is as a result filled by an outer shell electron, and the atom subsequently de-excites by emitting a characteristic x-ray or an Auger electron. In multi-elemental samples, each element can be traced and identified by referring to its characteristic x-ray lines. The study of x-rays produced by light ions bombardments has received a great impetus by the development of analytical techniques. Protons of energy 2 - 4 MeV are found to be the most suitable ionising agents to use for the PIXE principle as one of the leading multi-elemental analysis technique[16].

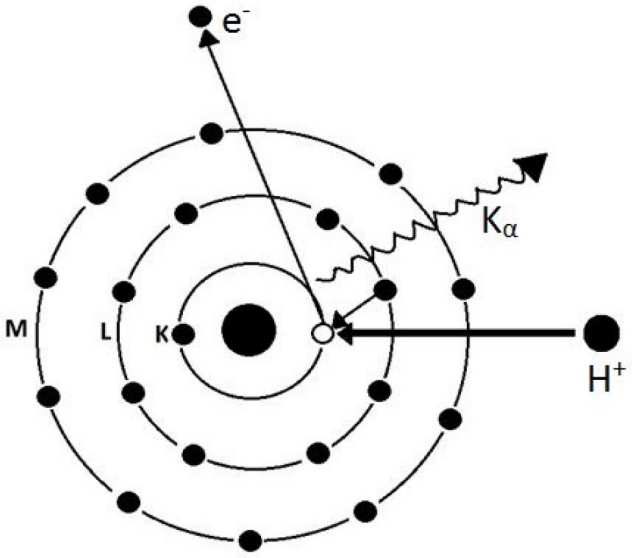

Figure 3: Characteristic X-ray Emission in an Atom.

PIXE has relatively high cross sections when compared to the other excitation processes. As a result, the characteristic x-rays are produced in abundance with relatively low background interference and only a small amount of sample's material is required for the analysis. If everything works well under good conditions, it is possible to detect 1-2 parts per million in quantity over a wide range of elements. The PIXE process is a non-destructive, non-invasive, no sample surface contamination, such as oxide layers and do not affect the analysis since PIXE is usually insensitive to elements with $Z < 13$. For thick target samples one is able to detect through a few micro-meter depth, which is the typical range of light ions in solids, taking into account the energy loss of the ion and self absorption effects.

2.3 Background spectrum

The main sources for continuous background radiation in the low energy PIXE spectrum are atomic bremsstrahlung (AB), secondary electron bremsstrahlung (SEB) and quasi-free electron bremsstrahlung (QFAB). These continuous backgrounds mainly determine the limit of detection in PIXE spectrum by underlying the characteristic x-ray peaks. In the case of elements with $Z < 35$, the detection limit of PIXE is determined by SEB, AB and QFAB background components [17]. SEB and AB are the main components in the low energy PIXE spectrum [18]. Other components forming the background are nuclear bremsstrahlung (NB) and the Compton tail of γ-rays, which is produced by the nuclear reactions.

2.3.1 Atomic Bremsstrahlung

Atomic bremsstrahlung are from Coulumbic interaction of the incident projectile particle with the bound electrons in the target material. The inner shell electron of the target material becomes excited from the interaction with the projectile. The electrons then de-excite by proton emission, the emitted proton are continuum because they are coming from different depth of the target material, they experience lose of energy on there way travelling through the material. Photons coming from different depths lose different amount of energy and hence the continuum spectrum.

Atomic Bremsstrahlung cross-section equation can be obtained by using PWBA theory and hydrogen-like wavefunction [18]:

$$\frac{d\sigma^{AB}}{d(\hbar\omega)} = \frac{8a_o^2\alpha^5}{\pi\hbar\omega}Z_p^2\left(\frac{c}{v_p}\right)^2\frac{\int_\omega^\infty}{v_p}\frac{dq}{q}\times\left\{1-\left(\frac{\omega}{qv_p}\right)^2+\left[\frac{3}{2}\left(\frac{\omega}{qv_p}\right)^2-\frac{1}{2}\right]sin^2\theta_L\right\}\times|Z_pS\ (Z_T,q)\ |^2 \tag{1}$$

Where $\hbar\omega$ is the energy of the photon, a_o is the Bohr atomic radius, α is the fine-structure constant, Z_p is projectile's atomic number, Z_T is target's atomic number, c is the speed of light in vacuum, v_p is the velocity of the projectile, θ_L is photon emission angle with respect to the incident projectile direction.

2.3.2 Secondary Electron Bremsstrahlung (SEB)

The incident nuclei has enough energy to eject an electron from the shell of the target material's atom. this free ejected electron then interacts with the target's nuclei coulomb field while travelling through the target material, it then gets scattered and loses energy thereby emitting a secondary electron bremsstrahlung.

The cross-section of secondary electron bremsstrahlung (SEB) can be obtained by using BEA theory for the electron ejection cross-sections, PWBA equation for electron bremsstrahlung and Bethe equation for the energy loss [18].

$$\frac{d\sigma^{SEB}}{d(\hbar\omega_L)} = \frac{1}{2\pi}Z_P^2\left(\frac{e^2}{\hbar}\right)^5 a_o^2 Z_T\frac{m_ec^2}{(\hbar\omega)^2}(C_1+C_2sin^2\theta_L) \tag{2}$$

The values of C_1 and C_2 can be gotten from literature[19], SEB can also be used for characterisation as shown in [17].

If V_p is projectile's velocity and T_m is the maximum energy which the projectile can transfer to a free electron at rest. Then, at energy above T_m, the intensity of secondary electron bremsstrahlung decreases very quickly. This happens because there are many more free and outer-shell electrons than inner-shell electrons and the bremsstrahlung energy higher than T_m is produced by the target atom's ejected inner-shell electrons.

$$T_m = 2m_e V_p^2 \tag{3}$$

2.3.3 Quasi-free Electron Bremsstrahlung (QFEB)

The Quasi-free electron bremsstrahlung (QFEB) are created when the velocity of the projectile particle is much greater than that of the orbiting electrons of the target material's atom. Considering this from the angle of relativity the target electrons are considered to be free electrons in the frame producing QFEB.

$$\frac{d\sigma^{QFEB}}{d\omega d(\hbar\omega)} = \frac{N_\tau}{\pi} Z_P^2 \left(\frac{e^2}{\hbar}\right)^5 a_o^2 \frac{m_e c^2}{T_r \hbar\omega} \times \left[sin^2\theta + \frac{1}{4}(1+p^2)(3cos^2\theta - 1) In\left(\frac{1+p}{1-p}\right) - \frac{1}{2}p(3cos^2\theta - 1)\right] \tag{4}$$

Considering the relativistic relationship $p^2 = 1 - \hbar\omega/T_r$ and that the number of electrons of the target atom is N_τ. The energy spectrum of QFEB can be characterized by the relativistic kinetic energy T_r[20].

where;

$$T_r = \frac{m_e E_P}{M_P} \tag{5}$$

2.4 Quantitative Analysis

In other to conduct a very good estimation of the elemental presence in the sample, we have to put into consideration the classical events happenings at atomistic level. In addition to the X-ray production probability, the composition of the target has influence on particle energy loss and X-ray attenuation as well. Mostly the PIXE characteristic X-ray yield of a particular element in a sample towards a detector can be represented as;

$$Y_i = \int_0^d c(x)\sigma_i(E(x))e^{-\mu x/cos\theta} dx \tag{6}$$

The projectile particles lose their energies travelling through the sample with this equation:

$$E(x) = \int_0^x S(E)dx \tag{7}$$

where;

$$S(E) = \frac{dE}{dx} \tag{8}$$

If the element $i-th$ happened to have a constant concentration profile c(x) and the X-ray detector has an efficiency ε the relationship between the observed X-ray intensity and element concentration is given as;

$$I_i = QC_iK_i \tag{9}$$

K_i is the calibration constant which is independent of the sample, if both geometry of the experiment and sample matrix composition do not change. It is given as;

$$K_i = \varepsilon \int_0^d \sigma_i(E(x))e^{-\mu x/cos\theta}dx \tag{10}$$

Looking at Eqs (9) and (10) It is clear that for a reliable PIXE analysis, several conditions have to be fulfilled. Successful analysis can be performed on well-characterised sample (flat surface, known thickness and matrix composition), and fully controlled experimental conditions (in case of thin samples, analysis is much simplified).

For the quantification procedure, one can either use the fundamental parameter approach by calculation of K_i from X-ray production cross sections σ_i, particle stopping power S(E) and X-ray attenuation μ or by comparing data of unknown sample with the that of already known standard samples, so calibration constant K_i can then be deduced. The most important parameters where the presence uncertainties can influence the precision, accuracy and outcome of PIXE as analytical technique are the following:

- particle energy (E_o),
- total exposure of sample by incoming particle beam (Q),
- geometry (θ, Φ),
- detection efficiency (ε),
- matrix composition,
- statistical uncertainty in the determination of peak area I_i.

A direct elemental concentrations in the sample can be obtained from PIXE spectra using the following equation if all other parameters are known.[2]

$$dN = A(s)n(s)\sigma\omega k\Omega T\varepsilon dS \tag{11}$$

Defining all the parameters we have;

dN = number of counts coming from the sample
A(s) = atoms in the sample's surface element of dS
n(s)= total number of protons in area of cm^2 travelling through same surface element
σ = ionization cross section
ω = fluorescence yield
k = probability for relative transition
Ω = solid angle
ε =detector's efficiency

T = transmission through irradiation chamber window

Integrating over the whole of the sample, total number of counts N in the peak can be calculated. n(s) is kept as constant if beam density distribution is uniform. So, by integrating A(s) over the whole surface, following expression is derived:

$$N = An\sigma\omega k\Omega t\varepsilon \tag{12}$$

The values of N for each peak can be obtained by using computer program experimentally, by fitting of certain polynomial background model to spectrum and Gaussian to each peak.

2.5 The Theory Volcanoes

Volcanoes are found in many different shapes and sizes, these are ranging from common cinder cone volcanoes that build up from several repeated eruptions and lava domes that pile up on-top of volcanic vents to form a broad shield volcanoes and composite volcanoes. The major determinant factor on what the shape of volcano would be is the viscosity of the molten magma. All volcanoes differ in terms of structure and appearance but they all share something in common; They are all awesome forces of nature and their eruptions leave significant effects on the environment. A good diagrammatic description of different parts of Volcano and events and what is going on within it is shown in Figure 4 below.

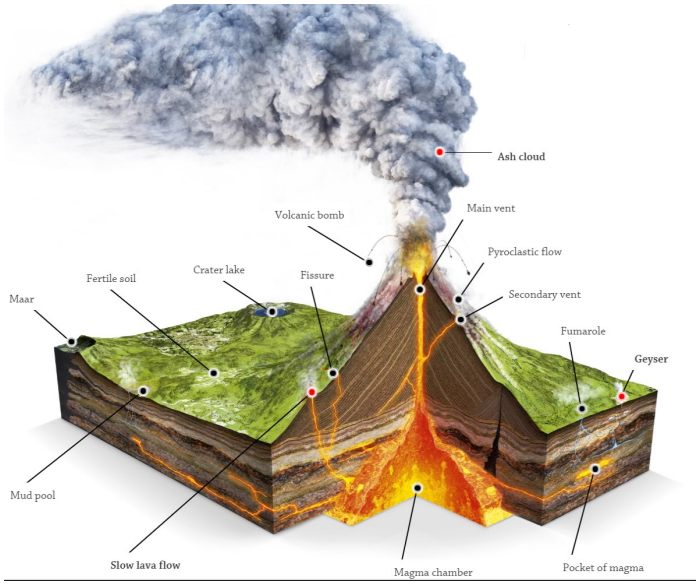

Figure 4: Volcanic Eruption Illustration [28].

All the volcanic activity comes down to the same basic principle. In other words, all volcanic eruptions that occur are as a result of magma movement from beneath the Earth surface being pushed up to the surface where it erupts as lava, ash and rock. In other to understand the mechanisms behind this process. We need to ask, exactly that makes molten rock rise from the Earth's interior layers and explode onto the landscape.

To get a good picture of how volcanoes eruption occurs, there is need to first put the structure of the Earth into consideration.

2.5.1 The Earth's Structure

At the very top is the lithosphere, the outermost layers of the Earth that consists of the upper mantle and crust. The crust makes up the outermost layer of the Earth, its thickness ranges from 10 km on the ocean floor to a maximum of 100 km in mountainous regions. It is the coldest and and most rigid part of the Earth and it

is primarily mainly composed of silicate rock. These various parts are shown in the figure 5 below.

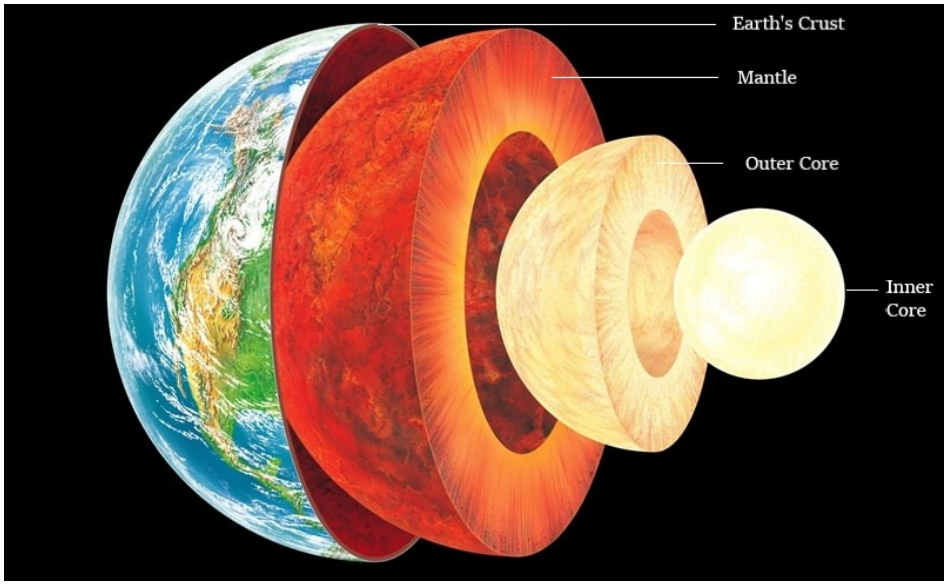

Figure 5: The Earth's Inner Structure[29].

The layer beneath the Earth crust is the Earth's mantle which is divided into sections of varying thickness based on their seismology. These sections are two sub-layers basically: the upper and lower mantle. The upper mantle extends from a depth of $735km(4.3to21.7mi)$ to $410km(250mi)$; there is however a transition zone between the upper and the lower mantle, which ranges from $410660km(250410mi)$; the lower mantle thickness ranges from $6602,891km(4101,796mi)$; and the core−mantle boundary, which is approx. $200km(120mi)$ thick on average.

Conditions change drastically in the mantle region compared to the earth crust. There is a considerable Pressures and temperatures increase. The temperature can easily reach up to 1000^oC, which certainly makes the rock become molten and viscous enough that it behaves like a liquid. This viscous molten rock flows into vast chambers of magma reservoirs beneath the Earth's crust as can be seen in Figure 4.

Since this magma is less dense than the surrounding rock, it's buoyancy is increased and it "floats" up to the surface, seeking out cracks and weaknesses in the mantle. When it finally reaches the surface, it explodes from the summit of a volcano. When it's beneath the surface, the molten rock is called magma but the moment it reaches the surface, it erupts as lava, ash and volcanic rocks.

With each eruption, rocks, lava and ash build up around the volcanic vent. The nature of the eruption depends on the viscosity of the magma. When the lava flows easily, it can travel far and create wide shield volcanoes. When the lava is very thick, it creates a more familiar cone volcano shape (a cinder cone volcano). When the lava is extremely thick, it can build up in the volcano and explode (lava domes).

Another mechanism that also drives volcanism is the motion the crust undergoes. To break it down, the lithosphere is divided into several tectonic plates, which are constantly in motion at the top of the the mantle layer. Sometimes these plates can collide, pull apart, or slide alongside each other; resulting in convergent boundaries, divergent boundaries, and transform boundaries. This activity is what drives majority of all geological activity, which includes earthquakes and volcanoes.

In the case of the volcano, subduction zones are usually the result, where the heavier plate slips under the lighter plate forming a deep trench. This subduction changes the dense mantle into buoyant magma, which rises through the crust to the Earth's surface. Over millions of years, this rising magma creates a series of active volcanoes known as a volcanic arc.

In summary, volcanoes are driven by pressure and heat in the mantle, as well as tectonic activity that leads to volcanic eruptions and geological renewal. The prevalence of volcanic eruptions in certain regions of the world such as the Pacific Ring of Fire also has a profound impact on the local climate and geography. For example, such regions are generally mountainous, have rich soil, and periodically experience the formation of new landmasses.

2.5.2 Volcanic Gaseous Emission

Volcanic magma contains dissolved gases, which provide the driving force that causes most volcanic eruptions. As magma rises towards the surface and pressure decreases, gases are released from the liquid portion of the magma (melt) and continue to travel upward and are eventually released into the atmosphere. Large eruptions can release enormous amounts of gas in a short time. The 1991 eruption of Mt. Pinatubo is thought to have injected more than 250 megatons of gas into the upper atmosphere on a single day. However, even if magma never reaches the surface, gases can often escape continuously into the atmosphere from the soil, volcanic vents, fumaroles and in hydrothermal systems.

By far the most abundant volcanic gas is water vapour, which is harmless. However, significant amounts of carbon dioxide, sulphur dioxide, hydrogen sulphide and hydrogen halides can also be emitted from volcanoes. Depending on their concentrations, these gases are all potentially hazardous to people, animals, agriculture, and property. As I mentioned before, 1991 eruption of Mt. Pinatubo is thought to have injected more than 250 megatons of gas into the upper atmosphere on a single day.

Carbon dioxide: Carbon dioxide constitutes approximately 0.04% of the air in the Earth's atmosphere. In an average year, volcanoes release between about 180 and 440 million tonnes of carbon dioxide. When this colorless, odourless gas is emitted from volcanoes, it typically becomes diluted to low concentrations very quickly and is not life threatening.

Sulphur dioxide: Sulphur dioxide is a colorless gas with a pungent odour that irritates skin and the tissues and mucous membranes of the eyes, nose, and throat. SO_2 emissions can cause acid rain. During very large eruptions, SO_2 can be injected to altitudes of greater than 10km into the stratosphere. Here, SO_2 is converted to

Figure 6: Mt. Pinatubo Eruption in Philippines on June 12, 1991 [30].

sulphate aerosols which reflect sunlight and therefore have a cooling effect on the Earth's climate. They also have a role in ozone depletion, as many of the reactions that destroy ozone occur on the surface of such aerosols.

Hydrogen sulphide: Hydrogen sulphide is a colorless, flammable gas with a strong, offensive odour. It is sometimes referred to as sewer gas. Interestingly, the human nose is more sensitive to H_2S than any gas monitoring instrument we have today: air mixtures with as little as 0.000001% H_2S are associated with a rotten egg smell.

Hydrogen halides: When magma ascends close to the surface, volcanoes can emit the halogens fluorine, chlorine and bromine in the form of hydrogen halides (HF, HCl and HBr). These species are all strong acids and have high solubility; therefore they rapidly dissolve in water droplets within volcanic plumes or the atmosphere where they can potentially cause acid rain.

Figure 7: Mt. Pinatubo's volcanic plume spreading out on the ground [31].

2.6 The Tree's annual rings

Trees have two types of growth: primary growth and secondary growth.

Primary growth occurs at the tips of roots and stems and results in their growing taller or longer.

Secondary growth takes place in the vascular cambium and the cork cambium and results in an increase in the diameter of the stem or trunk of the tree. Cambium lies between the old wood and the bark of the tree. The vascular cambium is a thin layer cells that produces conducting cells xylem and phloem.

The phloem is the outer layer, and is sometimes referred to as the inner bark. It is a food conducting tissue. **The xylem** is located towards the inside of the cambium layer.

The xylem is the vascular tissue through which most of the water and minerals of the tree are conducted. More secondary xylem (added towards the inside of the cambium layer) than secondary phloem (added toward the outside of the cambium layer) is produced by the cambium. The definition of wood is secondary xylem, reflected by the origin of the term 'xylem', the Greek word xylon, for wood.

Another layer, the cork cambium, contributes to the expanding girth of a tree. The cork cambium is a thin layer cells that ultimately produces the bark of the tree. The

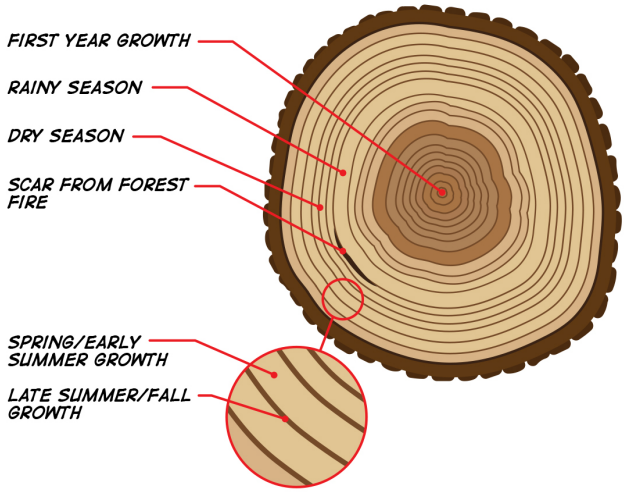

Figure 8: Tree Annual rings [32].

bark is composed of several types of tissue produced (both towards the inside and the outside of the tree) by the cork cambium layer. The development of a master tree ring dating system for any given site requires consideration of slope, temperature, age of the tree, precipitation, and other growth factors. Sometimes trees can produce 'extra' or 'false rings' in a year. Data from many individual trees are collected and standardized to eliminate variations that arise from isolated factors. By matching rings from older trees (dead or alive) with modern ones, researchers develop overlapping time spans extending farther back in time.

3 Experiment

3.1 The Accelerator Laboratory

The University of Helsinki's accelerator laboratory is located at Kumpula Campus of the university. It is under the physics department. This accelerator is built into the rocky ground, this helps a lot in eliminating noise interference that might be coming in from cosmic radiation into any experiment being carried out there. The accelerator lab has a 5MV TAMIA type accelerator on one side and a 500kV KIIA ion implanter on the other side. PIXE experiment is carried out on one of the beam lines connected to the 5MV TAMIA accelerator.

A simple diagrammatic layout of the lab is shown in the Figure 9 below.

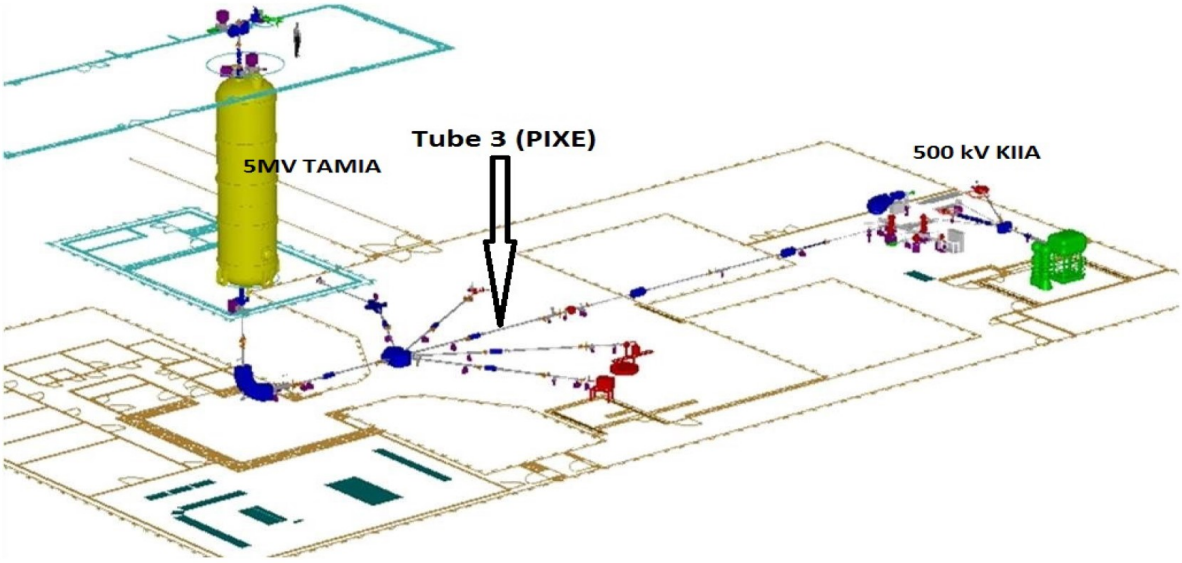

Figure 9: Kumpula Accelerator Laboratory Layout[33].

In Figure 4, the major components of the accelerator are illustrated, It shows from the point of ion production through the optics of ions transmission and acceleration up to the point of beam line and sample exposure.

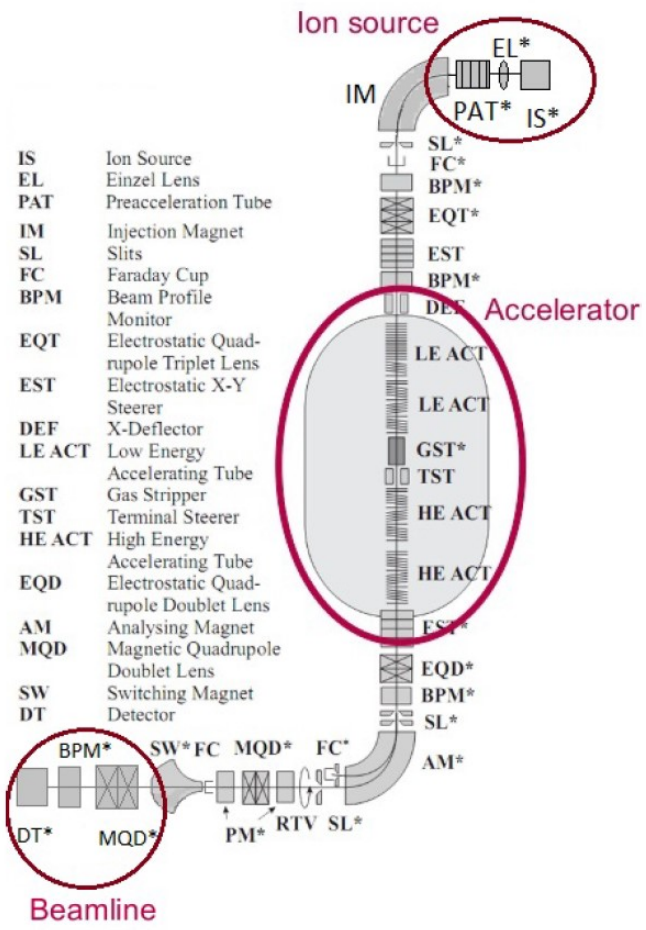

Figure 10: Beam transmission pat from Ion source through the accelerator [33].

3.1.1 Ion Source

Cesium Sputtering (SNICS) is a source of negative ions. It operates as a sputter ion source that is capable of delivering anions from a solid sample by bombarding it with Cs cations. Inside the discharge chamber of the ion source a reservoir of Cs is kept at high temperature to produce the vapour. A very hot conical ionizer is kept at a positive potential inside the chamber. The cathode used in SNICS is usually a Cs coated cylindrical section of Cu with a small cavity drilled onto the cylinder axis. This drilled cavity inside the cathode is filled with Powder of material from which the beam is desired while the whole set-up is maintained under a high vacuum. The vapour of Cs from the reservoir comes into the enclosed area between the cold cathode and heated ionizer. Some of the Cs adheres to the cool surface of the cathode while some hit the

hot surface of the ionizer and boils away immediately being ionized.

The ionized Cs then gets accelerated towards the cathode by the applied electric field and sputters atoms out of the powdered sample. Some materials preferentially sputter negative ions, while some sputter neutral or positive particles which pick up electrons while passing through the cold, condensed layer of Cs and produce negative ions. Since the entire ion source is operated below the ground potential and the extractor is kept at high positive potential with respect to the whole ion source, the negative ions are accelerated and extracted out of the source. Instead of a single cathode, now SNICS ion source with multi-cathode (MC-SNICS) is being used where 40 cathodes can be put together on a wheel and one can quickly switch to various cathodes containing different materials.[21]

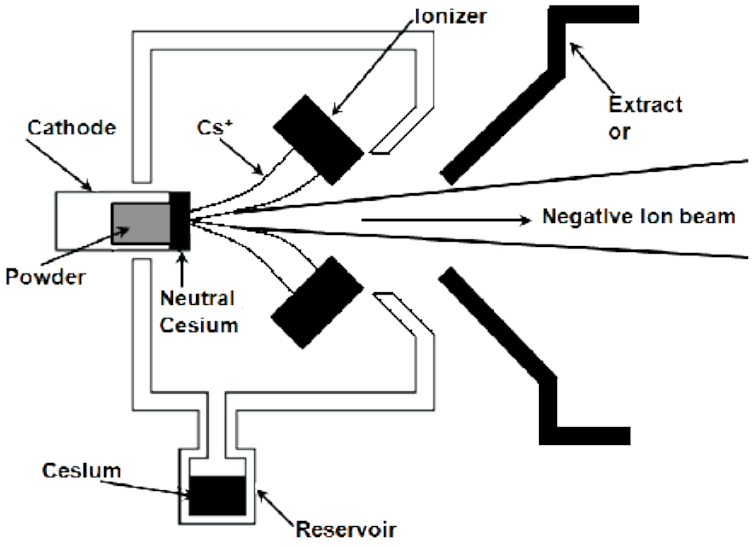

Figure 11: Cesium Sputtering (SNICS) Ion beam generation[34].

3.1.2 Acceleration of Ions

A tandem van de Graaff accelerator is then used to accelerate the ions generated in the ion source. In a van de Graaff accelerator, a moving belt transports charge to a high voltage terminal, which forms one end of an accelerating column. In tandem van de Graaff, the negatively charged ions produced by the negative ion source are accelerated from ground to the positive potential at the centre electrode of the accelerator. In the centre, the negative ions are stripped of electrons by passage through a foil or gas volume to become positive ions. After stripping, the positive ions are accelerated as they move from the positive potential on the centre electrode back to ground. This principle doubles the energy of the emerging beam for any given terminal voltage. The pressure vessel is often filled with an insulating gas. Because of its high reliability and

sufficient beam output SNICS sources are used extensively in tandem van de Graaff type accelerator, for example, the Pelletron. The drawback of SNICS lies in the limited time of operation before maintenance. After some days of use the cathode sample might be sputtered away and needs to be renewed. Also it cannot produce ion beams from the noble gases.

Figure 12: Accelerator tank [33].

Accelerator used for the measurements is located at the University of Helsinki's faculty of science, division of materials physics accelerator laboratory, in Kumpula Helsinki. Negative ions from the ion source are lead to the accelerator through the injection magnet. Accelerator used for the irradiation experiments was TAMIA 5 MV tandem Van De Graaff -accelerator EGP-10-II. It provided 3 MeV protons for this experiment. Acceleration tube is located inside the tank shown in Figure 12.

3.1.3 Beam Line

Beam is lead to the beam line through the analysing magnets, afterwards they pass through the collimator to keep the beam in focus as they approach the sample. Beam Profile Monitor (BPM), which is used to measure beam current, is placed in vacuum before the exit window where the beam enters the laboratory atmosphere. The ion beam can travel a few centimeter in the air after they exit the beryllium window that separates the vacuum environment within the accelerator set-up and the laboratory atmospheric condition.

3.2 External PIXE

There are two main types of PIXE, these are; **Internal PIXE** and **External PIXE**. They are both describing the environment where the sample is being irradiated. 'Internal' implies in an enclosure with controlled pressure, while 'External implies that it's in an opened environment such that of the laboratory environment. This work was actually done under the external PIXE condition.

Taken the measurements in open air has lots of advantages over the PIXE done in a closed vacuum environment. The nature of the sample in terms of shape, size, liquid content can play an hindrance in using internal PIXE approach. External PIXE brings a lot of ease to sample handling and also reduces the damage which can be created by heating on the sample surface at the beam spot. Air conventional current takes most of this heat away. PIXE measurement can be carried out on biological samples that contains water under atmospheric pressure so easily without any fear of damage unlike in the closed PIXE measurement.

Charging effect causes big amounts of bremsstrahlung radiation. That happens because when using positively charged ion beams, it builds a positive charge on the sample surface. External beam PIXE also removes the charging effects of insulating samples [22]. When potential is high enough, discharge occurs and electrons get high accelerations and produce background radiation. Usually, conductive coating is placed over the sample in vacuum to remove this effect but in air this is not necessary.

3.2.1 Exit Window

PIXE in the air comes with some disadvantages too, one is energy loss of the beam, which happens because of the exit window, and also beam's path in air reduces energy of the beam. There is an exit window which separates the low pressure system within the accelerator from the standard atmospheric pressure of the laboratory in which the sample is present. A very good example of this exit window is the Beryllium exit window. It has to be strong enough to withstand the pressure difference and thin enough so that the beam doesn't lose much energy when going through it.

The main purpose was to get maximum beam spot size with minimum exit window membrane thickness. With large beam spot size, it is possible to get high total beam current with low beam current density. For this experiment 0.5mm beam spot size was used, with this we could reduce the measurement time and get better detection sensitivity and also minimize the damage done to the sample by the beam. With the large beam spot size, one could get larger sample area hit by the beam without needing to move the sample to scan the surface.

Current measurement in external beam PIXE can also be problematic because the beam ionizes the path it travels in air. Then, when collecting the charge from the sample, electrons from the ionization path can cause error in current measurement.

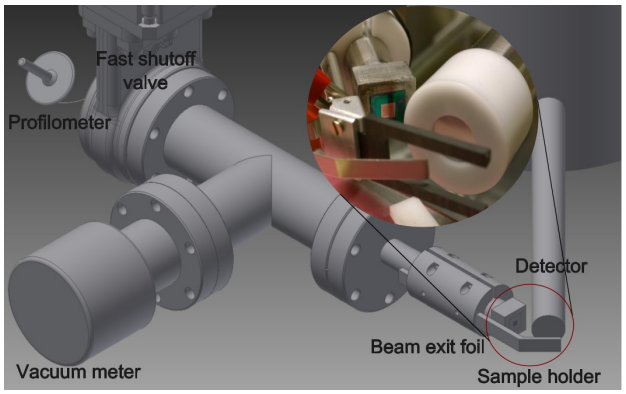

Figure 13: Layout of the external beam PIXE set-up.

3.2.2 Measurement Geometry

One thing that can also cause problems, is the fact that measurement geometry has to stay the same with every measurement and in external beam PIXE, set-up is in laboratory without any cover. One must be very careful not to change the geometry when switching samples[23]. The problem that could come with the geometry fluctuation was mitigated by the use of remotely controlled sample stage.

In Figure 13 above I try to show a model of our external beam PIXE principal component with profilometer to measure current, fast shut-off valve for vacuum protection, vacuum meter and close-up of the beam extraction window, detector and sample holder. In reality the sample holder we used was an adjustable remote controlled stage with allows you to take a long range of measurement without manually disturbing the whole experimental set-up.

Figure 14: Actual geometry Set-up of the experiment.

Here, in Figure 14, is the real set-up of the experiment, though this is an external PIXE measurement, the whole set-up is placed within a black box to remove interferences that might be coming in from light, this helps a lot in unwanted noise removal. The geometry of the beam exit window and the silicon detector drift is angled at 90^o. The sample itself is positioned at an 45^o to both of them. This geometry is maintained through the whole measurement and the distance between them are kept constant as well.

3.2.3 Detector and Electronics of the measurement

A **KETEK** Silicon Drift Detector (SDD) was used in this experiment. This detector is particularly suitable for detection of low energy trace elements. Since the elements of interest in this experiment belongs to this class of elements. Measurements were done with reverse bias voltage. Under reverse bias, an electric field extents across depleted region in P-N junction of the Silicon Drift Detector.

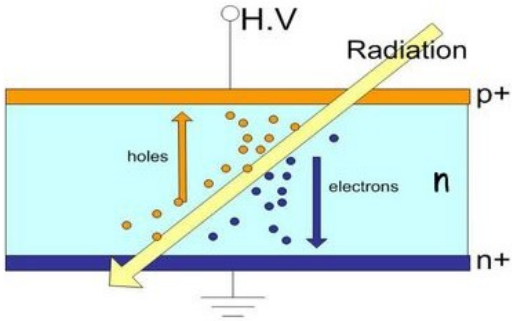

Figure 15: Charge carrier formation in SDD.

Charge carriers are produced in the form of holes and electrons pair when x-rays from the sample interact with the depleted material of the detector. The amount of Charge, which is collected by the electrodes is proportional to the energy received from the radiation. This charge carriers are migrated to the anode and cathode electrodes under the electric field. In other to have a good view of performance of this detector compared to other kinds of detectors, the following comparison was made with them.

These other detectors are namely Ultra LEGe detector and Si(Li) detectors. Each of this detectors have there moments of great advantage over one another. This can be more clearly put into perspective in Figure 16. Si(Li) detectors clearly perform better when we consider both world of high and low radiation energy detection. However, Ultra LEGe detector, does perform very well when it come to high radiation energy detection associated with heavier elements.

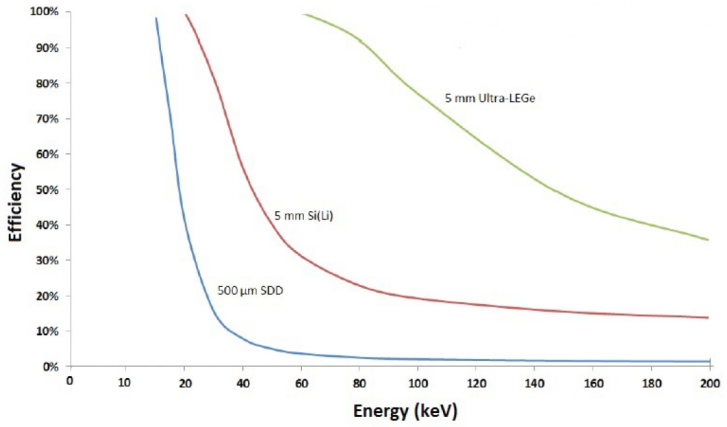

Figure 16: Performance comparison among the detectors [24].

The collected charge in the detector is converted to voltage pulse by a pre-amplifier. The pre-amplifier is connected to the amplifier and to high voltage power supply with coaxial cables. Linear amplifier is connected to Dual analogue-to-digital converter, which is then connected to the multi channel analyser (MCA) and to the computer. A simple connection discription is shown if Figure 17 below.

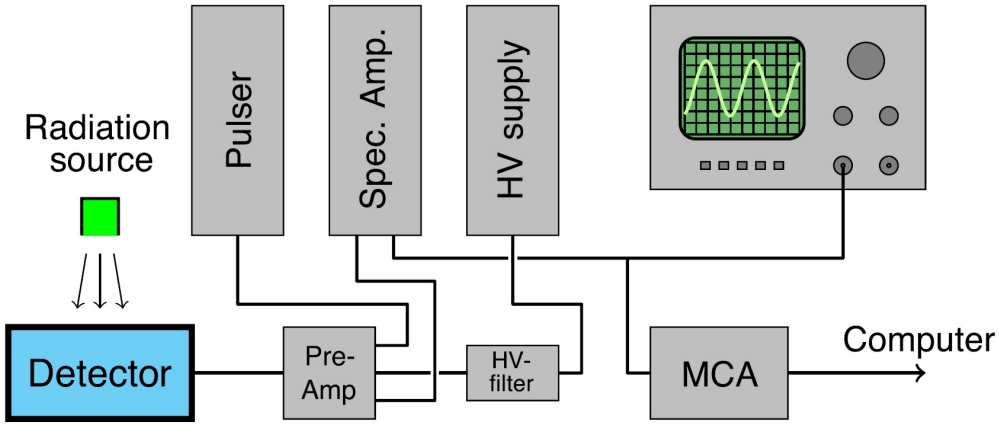

Figure 17: Detector electronics connections.

3.3 Samples and Measurements

The elemental quantification of each annual rings in each tree sample was determined using the external beam PIXE measurements. Each sample's annual year ring was irradiated for 400 seconds with stream of 3 Mev proton beam in our external beam set-up. X-ray spectra was acquired and saved for all the measurements. While taking these measurement there was constant keeping close tabs on the beam current, dead-time and beam aperture as all these play an important factor in the quality of the obtained spectrum.

Figure 18: Kumpula Accelerator Laboratory Control Unit

3.3.1 Samples and Sample Preparation

The samples were section of a sector of 2 different trees cut from different regions of Finland. For the measurements, they were neatly cut off from a bigger bulk of sector of the tree stem obtained just a couple of years back when the tree was fell. This small sector was first carefully polished on the surface to obtain a smoothness uniformity across the surface to be irradiated. Polishing this surface also makes it easier and clearer to see the annual tree ring formations clearly. Irradiating the surface without sand smoothing could easily affect the behaviour of the Ion beam on this sample surface.

After this, the sample is gently clamped into position on the sample stage. As mentioned earlier, the sample stage is remotely controlled from the work station after an initial position calibration as been done. This initial position calibration gives us knowledge of where the beam spot is located on the sample and that we are ionizing the right annual ring of that wood sample. Afterwards, we just continued to change the position of the beam spot(in order of mm) as we moved the beam spot along the sample

surface. As shown if Figure 19, the various stages of sample collection and preparation for irradiation.

(a) Cuttin of Irradiated sample from Bulk stem sector.

(b) Sand Smoothing of sample surfaces.

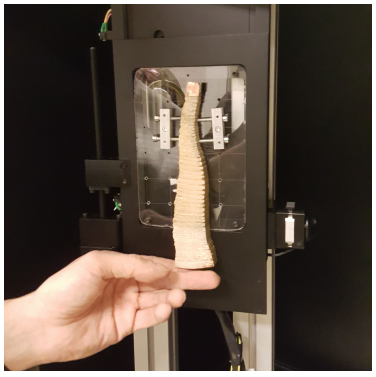

(c) Clamping of sample to sample stage.

Figure 19: Sample collection and preparation for Irradiation.

3.3.2 Analysis software PyMCA

The collected spectrum data was analysed in a software called PyMCA. PyMCA has been developed by the Software Group of the European Synchrotron Radiation Facility (ESRF). The name is from Python anguage which it written in and ofcourse MCA is for Multi- Channel Analyser. PyMCA is a ready to use, and in many aspects state-of-the-art, set of applications implementing most of the needs of X-ray fluorescence data analysis. PyMCA is use to interpret X-ray fluorescence spectra from a diverse array of samples. You can give PyMCA information about your experiment, and it makes a good estimate of the concentrations of the elements. PyMCA can be used to identify individual elemental contributions to complicated spectra, and can yield trace element concentrations with surprisingly good accuracy.

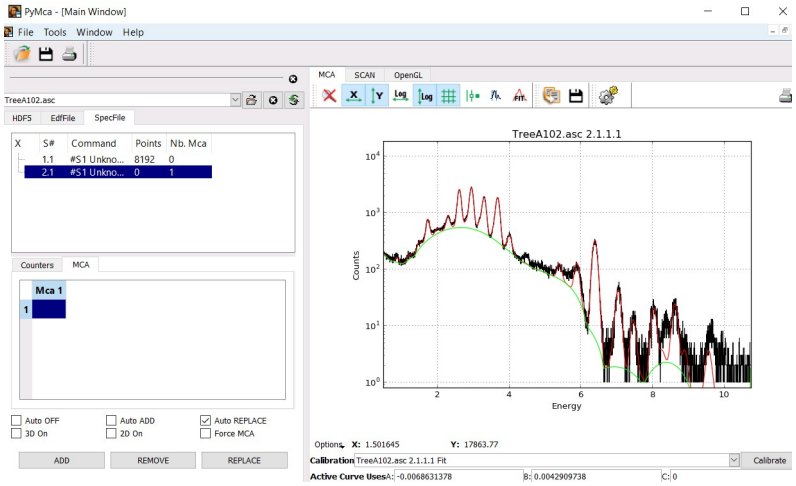

Figure 20: PyMAC software interface

Figure 20 shows the main interface of the PyMCA software, it is very well in support of many file types, most especially for Spec and EDF files. The software comes really quite handy has you only need to carry out your calibration of your channels just once and it is easy to compare this with the rest of the obtained spectra.

Figure 21 shows the peak fitting ability of PyMCA. The channels are linearly correspondent to the energies associated with each of the fitted peaks. Under the Table tab, you find the estimated area under the peaks of all elements fitted in the spectrum.

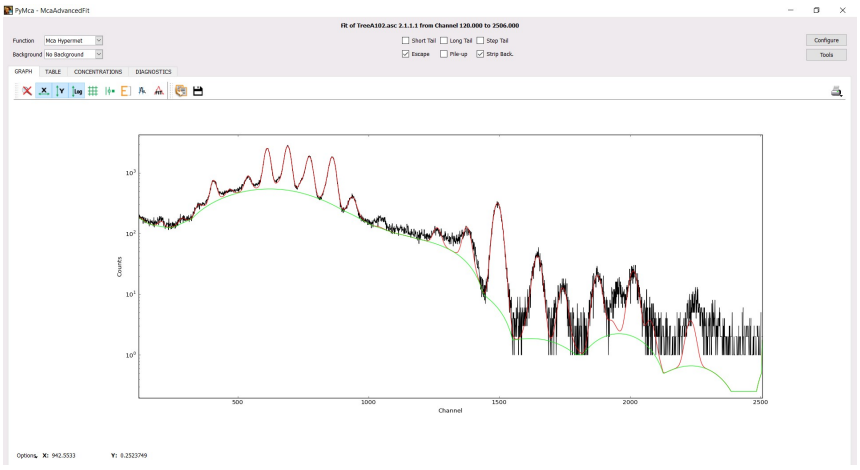

Figure 21: Kumpula Accelerator Laboratory Control Unit

4 Observations and Results

The whole experiment was done on the bases of elemental characterisation and quantification using a unique method of Ionisation to generate excitation of the element presents in the sample. The observed elements seen in these sample of trees are shown in Figure 22.

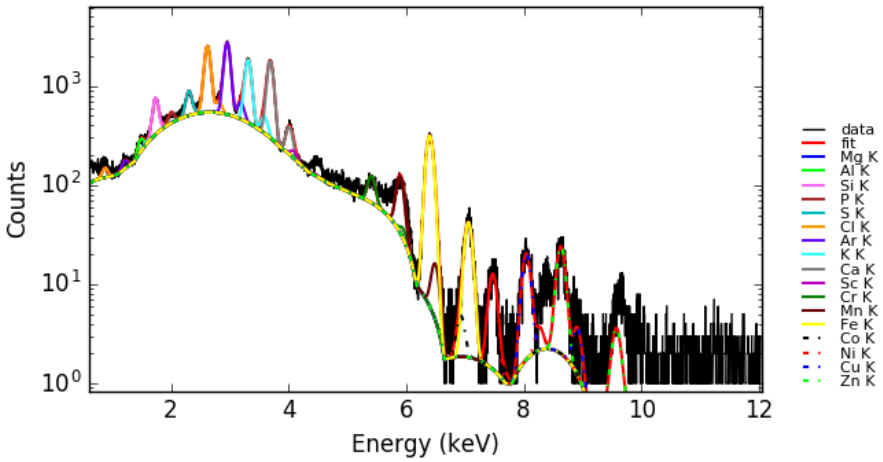

Figure 22: Identified elements in each of the spectrum

The two tree sample used for these experiment where gotten from two different regions of Finland. The first tree is a Pine tree from Parikkala(a small place near Savolinna) in the south-eastern part of Finland and the second tree is a Spruce tree from Pielavesi(place near Kuopio) in the central part of Finland. These locations are described in Figure 23.

As it can be seen in Figure 22 above the list of elements detected after characterisation are Mg, Al, Si, P, S, Cl, Ar, K, Ca, Sc, Cr, Mn, Fe, Co, Ni, Cu and Zn. The quantities of these elements found in each year of our samples varied considerably. In all the tree rings we measured, the area under the peaks found for each of these elements were normalised to the area found for that of Argon. The reason behind this is because the geometry for the measurements was kept constant throughout the whole process. This led to the assumption that the amount of Argon that exit in the air between the exit window and the sample constantly being detected in each of the year ring measurement is constant.

The first tree measured was the Pine tree and it is heavier and denser than the Spruce tree. The tree rings are also very well spaced in this tree for atleast an average distance of about 5mm to 7mm. This is suggestive that most the growing of this three was in a relatively humid environment. The tree density play a big role in observation we have, as high density sample implies that there is more cross-sectional interactions between

the incident beam and the sample target, this produces more transitioning electrons which in turn yield more characteristic x-rays.

Figure 23: Locations where samples were collected [Google maps]

4.1 Measurements in The Pine Tree

4.1.1 Chlorine and Sulphur Measurements in The Pine Tree

The two most prominent years of interest in this work are; The year 1991 and 2010, these are the 2 years we are hoping to see the volcanic effect of Pinatubo(1991) in the Philippines(because this is a category 5, which leaves a global effect) and the yjafjallajokull (2010) in Iceland (happened close to Finland). A good amount of Sulphur and Chlorine were found in these two particular year rings. The major sources of Chlorine and Sulphur in the atmosphere are the human activity like smelting and a natural volcanic eruption. In a study conducted on The Atmospheric Sulphur Cycle and the role of Volcanic SO_2, It has been found that volcanic emissions constitute 10% of the present-day global SO_2 source to the atmosphere, but form 26% of the SO_2 burden, and 14% of the sulphate aerosol burden. Two previous modelling studies suggested the volcanic fraction of sulphate was 18% and 35%, from sources representing 7% and 14%, respectively, of the global total SO_2 emission[24].

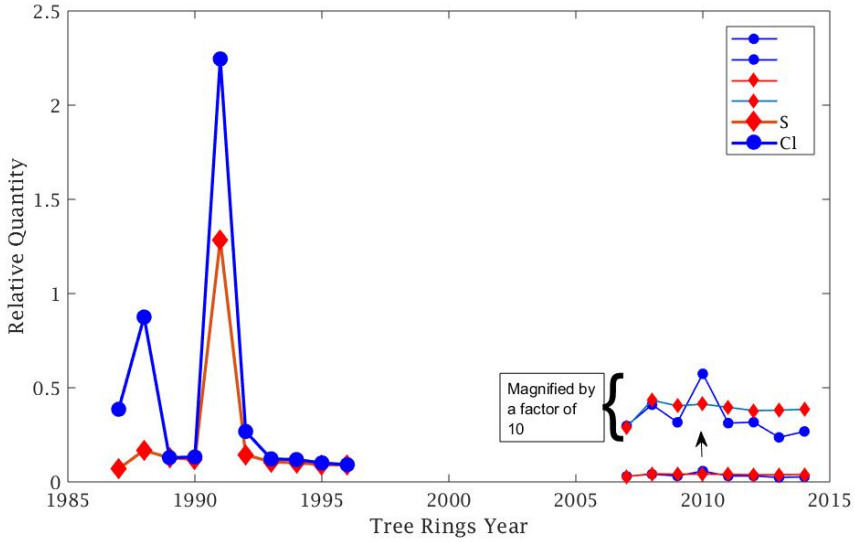

Figure 24: Pine tree's annual rings characterisation(Elemental Concentration per annual rings) for Sulphur and Chlorine.

There have been several recent detailed reviews of the global sulphur cycle (Rodhe, 1999; Penner et al., 2001), compiling results from a series of studies over the last decade (Langner and Rodhe, 1991; Pham et al., 1995; Chin et al., 1996; Chin and Jacob, 1996; Feichter et al., 1996; Graf et al., 1997; Chuang et al., 1997; Roelofs et al., 1998; Restad et al., 1998; Kjellstrm, 1998; Adams et al., 1999; Koch et al., 1999; Lohmann et al., 1999; Rasch et al., 2000; Barth et al., 2000; Chin et al., 2000).An illustration of the main features of the tropospheric sulphur cycle, and indicates fluxes, burdens, and lifetimes, and the average results of 11 models, as reported by the

Intergovernmental Panel on Climate Change (IPCC) is in their report (Penner et al., 2001).

The output of volatile chlorine during a major volcanic event can greatly exceed the annual man-made emissions of chlorine to the atmosphere. The fate of volcanic chlorine is particularly important since it has been argued that volcanoes may actually control the chlorine budget of the stratosphere, and hence contribute to ozone depletion. Large volcanic eruptions are capable of episodically injecting huge quantities of chlorine into the stratosphere, these Chlorine get dissolve is volcanic steam and atmospheric vapour. In the end, it ends up in the soil and plants.

The relative amount of Chlorine to Argon found in the Pine tree is seen in Figure 24 to be 2,246 and that of Sulphur is 1,283 for the year 1991, This is a significantly higher amount compare to the surrounding years before 1991 and after 1991. There was a clear continuous decline in the amount of these found immediately after the year of the event of Pinatubo. A significant amount of these where also noticeable in the year 2010, The chlorine gas was clear with an high value of presence, which I believe can be directly associated with the yjafjallajokull (2010) eruption in Iceland.

4.1.2 Cations Measurement in The Pine Tree

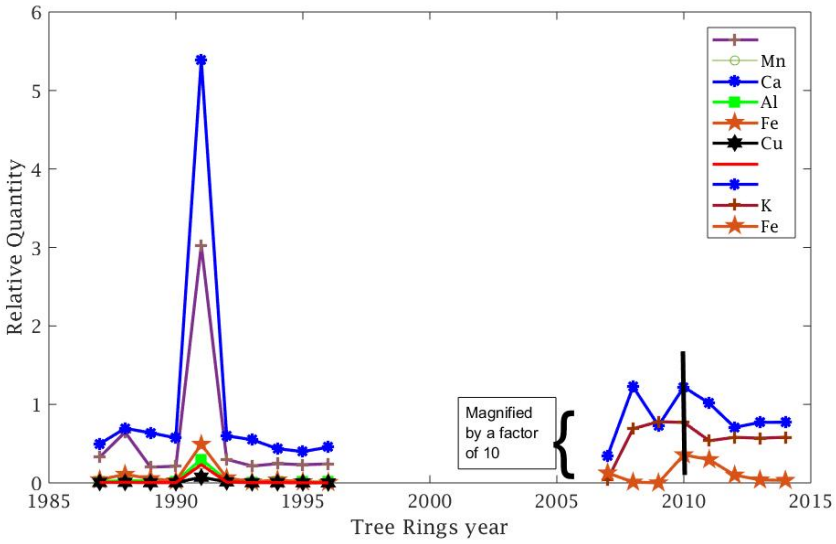

Figure 25: Pine tree's annual rings characterisation(Elemental Concentration per annual rings) for Cations

Alkali metals and alkali earth metals are natural reactant with chloride and sulphide ions. Figure 25 shows how this element have strong amount of presence in the tree

ring of 1991. Calcium has relative quantity ratio to Argon of 5,388 and potassium a value of 3,023. other elements that were found to show similar correlation to both sulphur and Chlorine are Mn, Al, Fe and Cu. A similar trend was also seen the 2010 tree ring.

4.2 Some Other Similar Work

There was a Boreal Environment Research 17: 128138 ISSN 1239-6095 (print) ISSN 1797-2469 (online) 2012, that did a similar project on measuring at atmospheric concentration of Sulphur and Chlorine. The Title of the work was "Comparison of atmospheric concentrations of sulphur and nitrogen compounds, chloride and base cations at Ahtari and Hyytiala, Finland". Just like the Title said, they did a Seven-year (2003 to 2009) time series of atmospheric SO_2, $SO_4{}^{2-}$, $NO_3{}^{-}$, $NH_4{}^{+}$ and Cl^{-} concentrations as well as four-year time series of atmospheric Na^{+}, K^{+}, Ca^{2+} and Mg^{2+} concentrations from Ahtari and Hyytiala background stations in southern Finland, located within 85 km of each other were compared.

Figure 26: Air sampler for measuring atmospheric gaseous concentration [26].

At Ahtari, the area within a 1-km radius around the sampling platform consists of forest, a lake, wetlands and arable land. The fields are located in the south-western sector. At Hyytiala, the 1-km radius surrounding the sampler mainly consists of forest and a lake, while a small field is located in the southern sector and the proportion of wetlands is low.

The measurement data used in this study were collected by the Finnish

Meteorological Institute (FMI) from two background stations in southern Finland. In there result the correlations between the concentrations of chloride, sodium, calcium and magnesium at the two stations were also very strong (rP = 0.83 to 0.89), showing a good correspondence between the stations. A significant, decreasing trend was found for all the sulphur and nitrogen components and chloride at both stations.

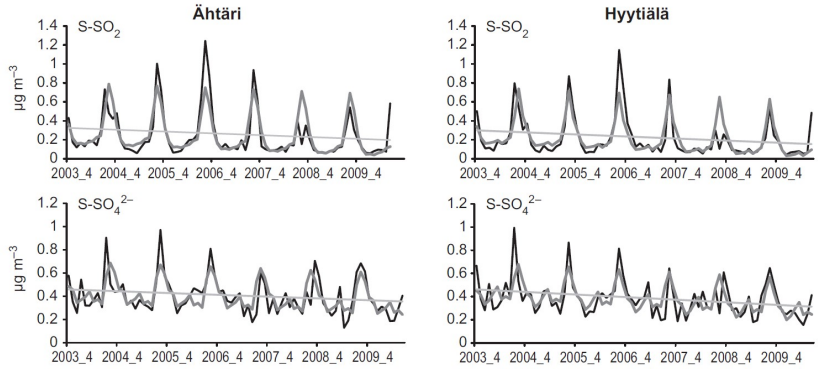

Figure 27: Their observed trend in atmospheric Sulphur gaseous concentration [26].

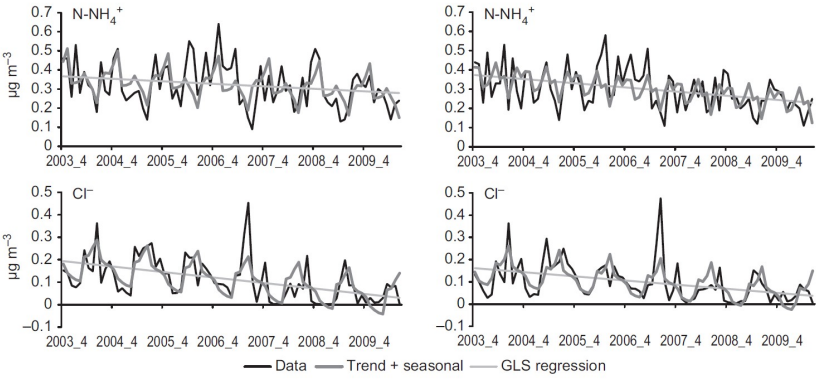

Figure 28: Their observed trend in atmospheric Nitrogen and Chloride gaseous concentrations [26].

These observations show a good agreement with our observations in the Pine tree. The location of the Ahtari station is quite close to that of location where the Spruce tree in our work was taken from in the central part of Finland.

4.3 Measurements in The Spruce Tree

Figure 29: Spruce tree rings and measurement.

Figure 29, shows the exact sample of the spruce tree that was irradiated in the measurement. At single glance at it, it clearly shows how closely packed the tree rings are, how low densely it is, it might be a bit hard to see from the image, but its sure has a lower density compared to the pine tree earlier measured.

4.3.1 Chlorine and Sulphur Measurements in The Spruce Tree

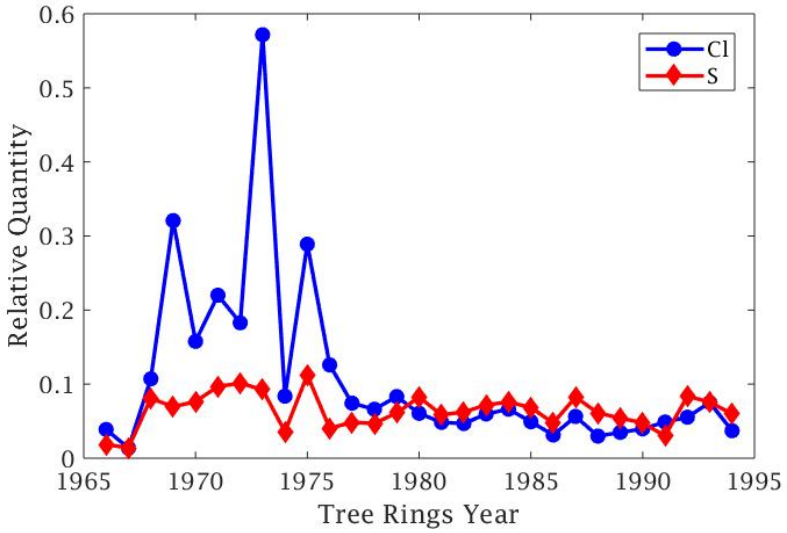

Figure 30: Spruce tree rings S and Cl measurements.

The window of measurements done on this sample span between 1966 and 1994, the trend and pattern seen in this tree shows a some activity involving cl and S between the period of 1968 and 1977, unfortunately I do not have an exact explanation for this. It could be as a result of local farming activity, but our main interest dwells on the effect of volcanic activities and this measurement just included the year 1991, in which Pinatubo occurred.

4.3.2 Cations Measurements in The Spruce Tree

Comparing what was seen in Figure 30 with what can be seen for the cations trends in spruce tree, there is very little correlation between the Chloride and Sulphide compared with that of the Alkali and Alkali earth metals is the tree rings. The major correlation is seen between the year 1968 and 1977, but Calcium and Potassium shows what would be expected around the year 1991 to 1994, a very high amount of presence.

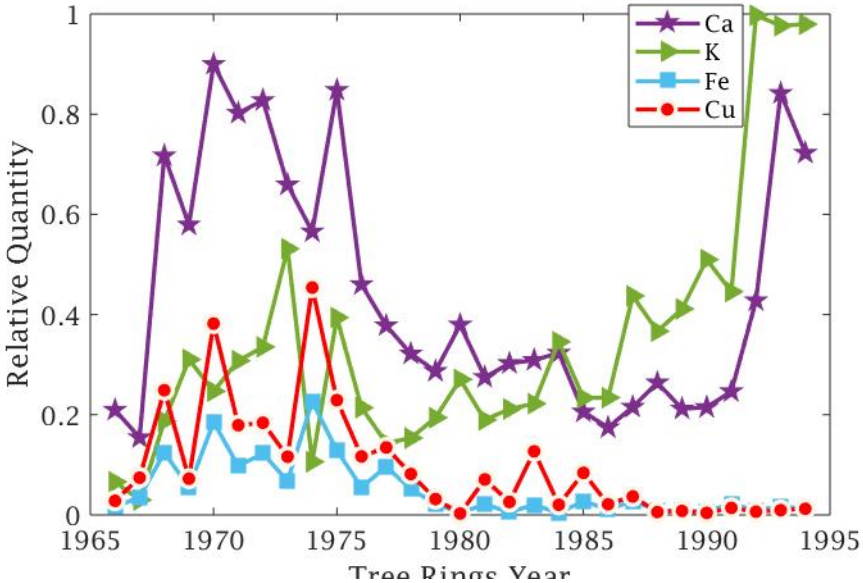

Figure 31: Spruce tree rings Ca, K, Fe and Cu measurements.

4.3.3 Measurements of Other Less Reactive Elements in The Spruce Tree

Further comparison of trend between similarly behaving element found in the tree ring sample, Silicon and Aluminium shows close behaviour between the year 1967 and 1977 but shows an inverse correlation beyond this years. The Silicon grew in quantity while the Aluminium diminishes. At around 1993 silicon has its highest value.

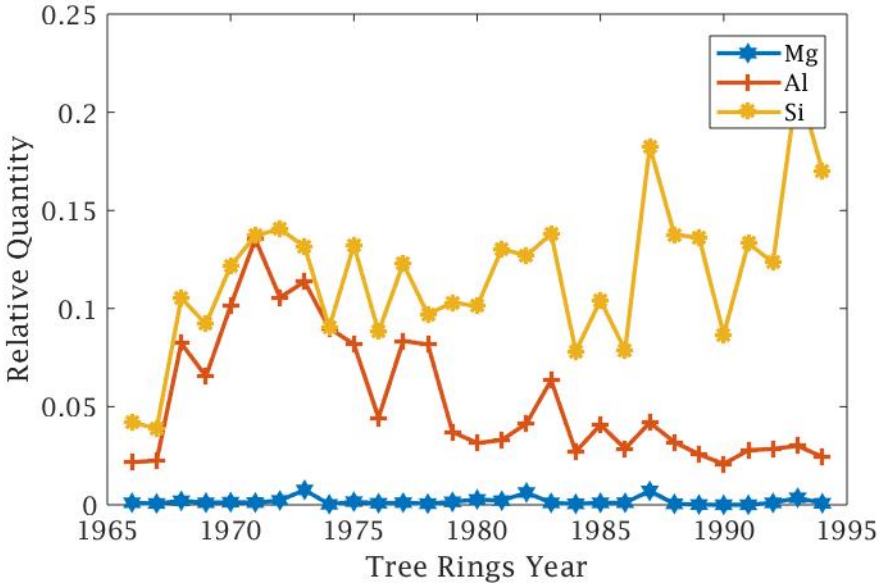

Figure 32: Spruce tree rings Mg, Al and Si measurements.

Figure 33, shows how Magnesium a similar trend as seen in earlier in Potassium and Calcium. Though the quantity of Magnesium found here are quite small but it still shows the correlation that you would expect for the presence of Chloride and sulphide.

I Strongly believe the nature of the sample measured here shows a difference in the outcome of the result seen in spruce tree compared to pine tree. The rings formations suggest a big difference in the humidity of the environment both trees grew in. The rings in the spruce are closely parked while that of pine are very wide spaced. The density of both tree sample are a lot different too, the spine has lower density compared to the spruce.

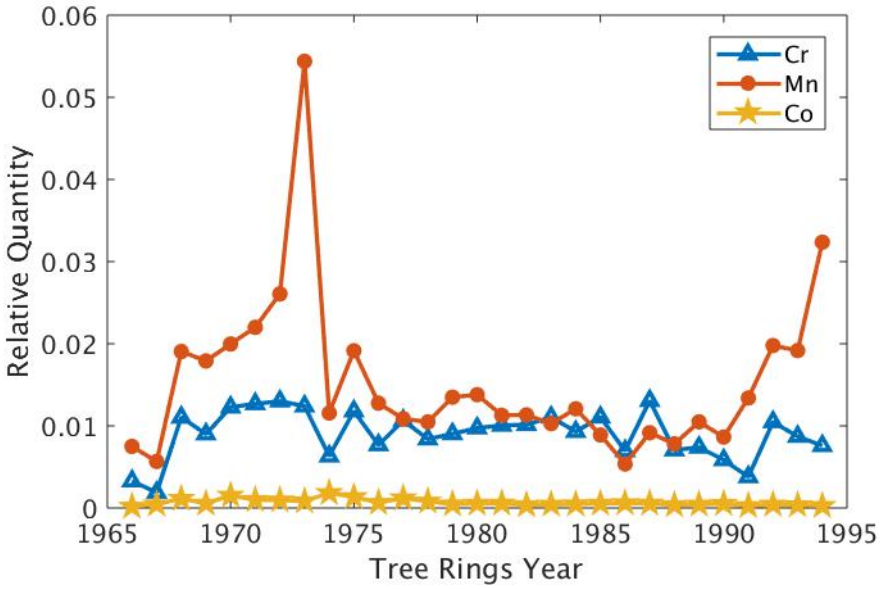

Figure 33: Spruce tree rings Cr, Mn and Co measurements.

5 Conclusions

This experiment was carefully carried out in the laboratory, there was a meticulous selection of samples to be used and the measurement to be done were carefully thought through. The two trees used were from the Pine (from the south-eastern Finland) and the Spruce(from the central Finland). Mount Pinatubo eruption received a special attention in this work because it is the second biggest volcanic eruption in history. It has the capability of altering the global climate and its magnitude was huge enough to leave its signature in almost all countries of the world. Eruption of yjafjallajokull, 2010 in Iceland receives attention though because of its closeness to Finland.

As explained earlier already, the tree rings are good way of getting events that happened in the past, several methods of extracting this information has been employed, from chemical analytic methods to various other physical methods. The method of ion beam is relatively new compare to these all other methods, though it holds a great potential if fully perfected. it gives detail information about constituted elements within the sample material at a single measurement.

The theory of this work explained how the ion beam interacts with a sample material. The nature of the outcome from this interaction has directly depends on the physical structure of the sample. A solid rigid and densely parked like the pine tree sample produces more inter-atomic interactions with the incident ion beam, the ion beam creates more cross-section which give a more definitive characteristic x-rays. The density found in the spruce is much lower compared with that of the Pine tree, this lower density result in ions travelling deeper into the sample before the are stopped, which implies more bremsstrahlung radiations.

The volcanic effect are more visible in the Pine tree, the peaks seen in Figure 24 and 25 are indicative of some volcanic activities within those year rings. The observations noticed in the Pine tree are further buttress by some other independent work that shows that there was a steady decline in the concentration of Sulphur and Chlorine in the atmosphere. Bearing, we are working with assumption that the atmospheric concentration of these gases is directly linked to the tree ring concentration that has been found in them.

The correlation between the Sulphur and Chlorine with metallic elements was quite good when they are compared with one another, especially for the year surrounding 1991 and 2010 in the first tree.

As explained earlier in section 2, introduction of large amount of Sulphur into the atmosphere can cause a drop in global temperature, Several eruptions during the past century have caused a decline in the average temperature at the Earth's surface of up to half a degree (Fahrenheit scale) for periods of one to three years. According to the Finnish Meteorological Institutes statistics, the mean annual temperature for the whole of Finland in 2010 was 1.3^{o}C, which is 0.6 degrees below the long-term average. The last equally cold year took place in 1987, when the annual mean temperature was 0.1^{o}C.

The annual mean temperatures for 2010 ranged from about 5^{o}C in Southwest

Finland to about 3^{o}C in Northern Lapland.

The average precipitation for the whole country was about 560 millimetres, which is about 30 millimetres less than normally. The highest annual precipitation was measured in the area extending from Southwest Finland to Kainuu, where rainfall locally exceeded 650 millimetres. The least rain was measured in Western Lapland, where precipitation was locally under 450 millimetres. When compared against long-term averages, the eastern parts of the country and the west coast received the least rain[27].

This unique climatic condition experienced in the year 2010, I believe has a direct connection to Icelandic volcanic eruption of 2010.

References

[1] David D Cohen, Grahame M Bailey, and Ramesh Kondepudi. Elemental analysis by pixe and other IBA techniques and their application to source fingerprinting of atmospheric fine particle pollution. Nuclear Instruments and Methods in Physics Research Section B: Beam Interactions with Materials and Atoms, 109:218-226, 1996.

[2] Johansson and Thomas B Johansson. Analytical application of particle induced x-ray emission. Nuclear Instruments and Methods, 137(3):473-516, 1976.

[3] Sven AE Johansson and John L Campbell. PIXE: A novel technique for elemental analysis, volume 47. Wiley New York, 1988

[4] Sven AE Johansson, John L Campbell, and Klas G Malmqvist. Particle-induced X-ray emission spectrometry (PIXE), volume 133. John Wiley & Sons, 1995.

[5] T. B. Johansson, K. R. Akselsson, S. A. E. Johansson. Nucl Instr Meth 1970, 84, 141.

[6] Jan Pallon,* Nathaly De La Rosa, Mikael Elfman, Per Kristiansson, E.J. Charlotta Nilsson and Linus Ros A new quantitative X-ray system for micro-PIXE analysis Copyright © 2017 John Wiley & Sons, Ltd. X-Ray Spectrom. 2017, 46, 319324

[7] INSTRUMENTATION FOR PIXE AND RBS IAEA, VIENNA, 2000, IAEA-TECDOC-1190, ISSN 10114289 © IAEA, 2000 Printed by the IAEA in Austria December 2000

[8] V Palonen, K Mizohata, T Nissinen, and J Risnen. External beam PIXE setup with large-area SiN window. Nuclear Instruments and Methods in Physics Research Section B: Beam Interactions with Materials and Atoms, submitted, submitted.

[9] E Holmqvist-Saukkonen, A. M Larsson, A Kriiska, V Palonen, K Mizohata, T Nissinen, M Oinonen, and Risnen J. Tracing grog, pots and neolithic baltoscandian corded ware culture contacts (sem-eds, pixe). In Program and Abstract Book. 40th International Symposium on Archaeometry. ISA 2014, May 19-23, 2014. Los Angeles, California, pages 41-42. Getty Conservation Institute, Cotsen Institute of Archaeology, University of California Los Angeles, 2014.
`http://ethnosalro.uaic.ro/download/ethnosalro`

[10] 10. J.H. Scofield, Phys. Rev. A 9 (1974) 1041.

[11] J.H. Scofield, Phys. Rev. A 10 (1974) 1507.

[12] M.H. Chen, B. Crasemann and H. Mark, Phys. Rev. A 21 (1980) 436.

[13] M.H. Chen, B. Crasemann and H. Mark, Phys. Rev. A 24 (1980) 177.

[14] M.O. Krause, J. Phys. Chem. Ref. Data 8 (1979) 307.

[15] J. L. Campbell, At. Data Nucl. Data Tables 85 (2003) 291.

[16] S.A.E. Johansson and J.L. Campbell, PIXE: A novel technique for elemental analysis, John Wiley and sons Ltd. (1988) U.K.

[17] K Murozono, K Ishii, H Yamazaki, S Matsuyama, and S Iwasaki. Pixe spectrum analysis taking into account bremsstrahlung spectra. Nuclear Instruments and Methods in Physics Research Section B: Beam Interactions with Materials and Atoms, 150(1):76-82, 1999.

[18] K. Ishii, H. Yamazaki, S. Matsuyama, W. Galster, T. Satoh, and Milos Budnar. Contribution of atomic bremsstrahlung in pixe spectra and screening effect in atomic bremsstrahlung. X-Ray Spectrometry, 34(4):363-365, 2005.

[19] A. Yamadera, K. Ishii, K. Sera, M. Sebata, and S. Morita. Quasifree-electron bremsstrahlung induced by the projectile field. Phys. Rev. A, 23:24-33, Jan 1981.

[20] K Ishii. High energy limit of atomic bremsstrahlung. Nuclear Instruments and Methods in Physics Research Section B: Beam Interactions with Materials and Atoms, 99(1):163-165, 1995.

[21] http://www.iuac.res.in/atmol/ safvan/mridulathesis/node14.html#fig:snics

[22] JF Dias, A Bulla, and M-L Yoneama. Charging effects in thick insulating samples. Nuclear Instruments and Methods in Physics Research Section B: Beam Interactions with Materials and Atoms, 189(1):72-76, 2002.

[23] T. Calligaro, J-C Dran, B. Moignard, L. Pichon, J. Salomon, and Ph Walter. Ion beam analysis with external beams: Recent set-up improvements. Nuclear Instruments and Methods in Physics Research Section B: Beam Interactions with Materials and Atoms, 188(1):135-140, 2002.

[24] Ultra-lege detector gul. http://www.canberra.com/products/detectors/pdf/ Ultra-LEGe-SS-C40696.pdf. Accessed: 2014-08-12.

[25] David S. Stevenson1, Colin E. Johnson2, William J. Collins2, and Richard G. Derwent2 1Institute for Meteorology, University of Edinburgh, Kings Buildings, Edinburgh, EH9 3JZ, UK. 2Climate Research, Meteorological Office, London Road, Bracknell, RG12, 2SZ, UK.

[26] Boreal Environment Research 17: 128138 2012 ISSN 1239-6095 (print) ISSN 1797-2469 (online)

[27] Finnish Meteorological Institutes
https://en.ilmatieteenlaitos.fi/press-release/125205

[28] https://www.sciencephoto.com/media/167743/view/composite
-volcano-erupting

[29] http://learnwise.co/layers-of-the-earth-diagram-to-label/
layers-of-the-earth-diagram-to-label-lovely-layers
-of-the-earth-maggie-s-science-connection/

[30] https://www.wired.com/2016/06/annotated-volcano-exploring-pinatubos-devastating-eruption-25-years-later/

[31] https://shvpl.info/imagemgkl-mount-pinatubo.htm

[32] https://climate.nasa.gov/internal_resources/1062

[33] Layout of accelerator laboratory. http://www.physics.helsinki.fi/tutkimus/mat/ionisadelaboratorio/ams. Accessed: 2015-05-09.

[34] https://www.researchgate.net/profile/Shoaib_Ahmad4/publication/324890969/figure/fig1/AS:622635453018112@1525459268399/Schematic-drawing-of-the-SNICS-source.png